Hindawi
Journal of Nanomaterials
Volume 2019, Article ID 5212938, 10 pages
https://doi.org/10.1155/2019/5212938

Research Article

Synthesis of Binary Bi_2S_3/ZnO Nanorod Array Heterostructure and Their Photoelectrochemical Performance

Asla A. AL-Zahrani,[1,2] Zulkarnain Zainal,[2,3] Zainal Abidin Talib,[4] Hong Ngee Lim,[2,3] Laimy Mohd Fudzi,[3] Araa Mebdir Holi,[5] and Mahanim Sarif @ Mohd Ali[3,6]

[1]*Imam Abdulrahman Bin Faisal University, Eastern Region, Dammam, Saudi Arabia*
[2]*Department of Chemistry, Faculty of Science, Universiti Putra Malaysia (UPM), 43400 Serdang, Selangor, Malaysia*
[3]*Materials Synthesis and Characterization Laboratory, Institute of Advanced Technology, Universiti Putra Malaysia (UPM), 43400 Serdang, Selangor, Malaysia*
[4]*Department of Physics, Faculty of Science, Universiti Putra Malaysia (UPM), 43400 Serdang, Selangor, Malaysia*
[5]*Department of Physics, College of Education, University of Al-Qadisiyah, Al-Diwaniyah, Al-Qadisiyah 58002, Iraq*
[6]*Forest Product Division, Forest Research Institute Malaysia, 52109 Kepong, Selangor, Malaysia*

Correspondence should be addressed to Zulkarnain Zainal; zulkar@upm.edu.my

Received 21 March 2019; Revised 13 June 2019; Accepted 9 July 2019; Published 8 August 2019

Academic Editor: Miguel A. Correa-Duarte

One of the most effective strategies to improve the photoconversion efficiency in the photoelectrochemical cell is by using an assembly of heterostructures. To do so, a simple and inexpensive method, that is successive ionic layer adsorption and reaction (SILAR), is used to deposit the narrow band gap energy semiconductor Bi_2S_3 on ZnO nanorod arrays (NRAs) at different SILAR cycles. The obtained binary heterostructure thin films were characterized by using X-ray diffraction (XRD), UV-Vis Spectroscopy, field emission scanning electron microscopy (FE-SEM), energy dispersive X-ray analysis (EDX), Raman spectroscopy, high-resolution transmission electron microscopy (HRTEM), and linear sweep voltammogram (LSV) to prove the crystal structure, optical properties, band gap energy, morphological structure, composition of elements, and electrical properties. The XRD revealed that ZnO NRAs possessed a single wurtzite crystal structure while Bi_2S_3 possessed an orthorhombic crystal structure. The as-fabricated Bi_2S_3/ZnO heterostructure exhibited enhanced visible light absorption and charge separation efficiency of photoinduced electron-hole pairs. The band gap energy of binary heterostructure Bi_2S_3/ZnO NRAs is 3.11, 3.00, 2.33, 1.96, and 1.89 eV at 3, 5, 7, 9, and 11 SILAR cycles, respectively, confirming the substantial improvement of ZnO NRA optical properties. The highest photocurrent density has been achieved by 1.92 mA/cm^2 of Bi_2S_3/ZnO NRAs fabricated at 7 cycles, exhibiting sixfold enhancement compared to that of intrinsic ZnO NRAs (0.336 mA/cm^2). This impressive enhancement was ascribed to the significant improvement in morphological structure, crystallinity, and optical properties of heterostructure photoanodes. Significant improvement was achieved in the photoelectrochemical cell (PEC) performance attributed to the fast separation, low recombination rate, and low impedance of the photoinduced electron-hole pairs as shown throughout the electrochemical impedance spectra.

1. Introduction

The consistent consumption of accessible energy sources as well as the concern of exhaustion of current sources within rising environmental crisis has drawn many researchers to combat these issues by using an effective clean approach for water splitting to generate clean solar fuel and convert solar energy to chemical energy. To achieve this aim, metal oxide semiconductors are utilized as a photoanode in the photoelectrochemical cells. Among oxide-based semiconductors, ZnO is the most encouraging candidate due to its high earth plenty, nontoxicity, and unique physical and chemical properties for many photovoltaic applications [1]. Owing to the large band gap

energy of ZnO (3.37 eV), the electron-hole (e^-- h^+) pairs are formed when it is irradiated by ultraviolet (UV) light which represents merely (4%) of the entire solar light spectrum. However, in terms of existing energy, visible light and infrared light represent most of the solar spectrum with 43% and 52%, respectively, compared to UV. Therefore, modification of the ZnO nanostructure is a crucial step to utilize the abundant visible spectrum. Numerous efforts have been done to overwhelm the restriction of ZnO NR arrays, such as doping [2], reducing the size of crystal, and photosensitization of the surface of ZnO NR arrays using narrow band gap energy materials [3]. Although the doping approach is effective, it has several drawbacks, such as the following: (i) impurity can be introduced strongly which affect the e^-- h^+ pairs and might act as a recombination centre [4]; (ii) doping can also suppress the resistance of ZnO against corrosion, particularly when the dopants are transition metal ions [5]. On the other hand, the coating of organic dyes on ZnO is considered productive for photosensitization of ZnO, but the poor stability of dye which can expose to the oxidative degradation is still one of the main disadvantages of this technique [6]. Recently, many researches have reported that combination of ZnO NRs with narrow band gap semiconductors (NBGM), such as metal chalcogenide, might be a vital technique to enhance the performance of ZnO NRAs as working electrodes in photoelectrochemical cells (PECs) and speeds the separation of charge carriers, and consequently, high photoconversion efficiency has been achieved. Enormous researches have reported sensitization of ZnO nanostructure using inorganic chalcogenide semiconducting nanoparticles such as CdS [7], PbS [8], Ag_2S [9], Cu_2S [10], Cu_2O [11], CdSe [12], and Bi_2S_3 [13] by using different methods which show a diverse of potential applications and a noteworthy improvement in their performance compared with the intrinsic construction. Among the aforementioned narrow band gap energy materials, bismuth sulphide (Bi_2S_3) has been selected for the current study since it has narrow band gap energy (~1.3-1.7 eV) with high absorbance coefficient ($10^4\,cm^{-1}$) [3]. Hence, Bi_2S_3 is capable to yield visible light to infrared from the solar spectrum which is reflecting on the photoconversion efficiency of PECs. These excellent features make Bi_2S_3 an outstanding photoconductive semiconductor and a significant candidate for fabrication of photoelectrochemical cells [14], hydrogen sensing and biomolecule detection [15], sensors [16, 17], IR spectroscopy [18], and photodiode arrays [19]. Although Bi_2S_3 is an excellent visible active semiconductor, its electron-hole recombination is much faster due to its low band gap energy [20]. Hence, heterostructured semiconductor materials with two different energy level system play a vital role in accomplishing the effective (e^-- h^+) separation. The integration of Bi_2S_3 with ZnO can reduce the rate of recombination and enhance the visible light absorption and photoconversion efficiency throughout stepwise heterostructure [21]. The position of conduction band (CB) of Bi_2S_3 is higher than ZnO, so the photogenerated electron can be easily transported from Bi_2S_3 to ZnO. While valence band (VB) of Bi_2S_3 is higher than that of ZnO, so photogenerated hole can be transferred from ZnO to Bi_2S_3 smoothly. Moreover, the suitable band-aligned edge of ZnO with that of Bi_2S_3 (type-II heterostructure) encourages better carrier separation and charge transportation [21]. Many techniques have been used to fabricate the heterostructure photoanode in PECs, such as chemical bath deposition [22], solvothermal method [23], hydrothermal method [18, 20, 24, 25], successive ionic layer adsorption and reaction (SILAR) [26], and electrodeposition [27]. Among the abovementioned approaches, the hydrothermal method and successive ionic-layer adsorption and reaction method (SILAR) have attracted great consideration in recent years due to its simplicity during operation and capability for huge-scale manufacture. Therefore, the hydrothermal method has been selected for growing highly oriented nanorods of ZnO while the SILAR method has been used for fabrication of Bi_2S_3/ZnO NRs array heterostructure. Herein, this study is aimed at integrating Bi_2S_3 with narrow band gap energy with highly aligned orientated ZnO NRAs to enhance to photoconversion efficiency of ZnO NRAs as a photoanode in the photoelectrochemical cells. Various characterization techniques such as X-ray diffraction (XRD), UV-Vis Spectroscopy, field emission scanning electron microscopy (FE-SEM), energy dispersive X-ray analysis (EDX), Raman spectroscopy, high-resolution transmission electron microscopy (HRTEM), and linear sweep voltammogram (LSV) have been employed for characterizing the structure, morphology, and optical and electrical properties of the binary heterostructure.

2. Materials and Methods

2.1. Synthesis of ZnO Nanorod Arrays. Highly orientated perpendicularly ZnO nanorods were grown on conductive indium tin oxide (ITO) substrate using a simple hydrothermal method. In brief, the coated ZnO seed layers on ITO substrates, which were prepared by sol-gel spin coating, were dipped upside down facing the wall of sealable glass vials containing approximately 20 ml of the prepared growth aqueous solution. The hydrothermal growth solution consists of equimolar of zinc nitrate $Zn(NO_3)_2$ and hexamethylenetetramine (HMTA, $C_6H_{12}N_4$) at the concentration 0.04 M, and the pH value was 6.5. The vials were loaded into preheated silicon oil bath at 110°C for 4 hours as described in the earlier work [9].

2.2. Preparation of Bi_2S_3/ZnO Nanorod Arrays. In this technique, the precoated hydrothermally grown ZnO NRAs on ITO glass substrate are subjected to SILAR adsorption steps. In the first step, the coated ZnO thin film was immersed in the cationic solution, which contains 3 mM of bismuth nitrate $Bi(NO_3)_3{\cdot}5H_2O$ (Sigma-Aldrich, 99%) for 60 sec. In the second step, coated ZnO NRs from the initial step were dipped in deionized water (DIW) for 60 sec to remove unadsorbed (loosely bond). In the third step, the resultant was dipped in the anionic solution consisting of 30 mM of Na_2S (FLAKE) for 60 sec followed by DIW rinsing for 60 sec [26]. These four steps produced one cycle and were repeated 3 to 11 cycles to study the effect of SILAR cycles on

the morphological structure, optical properties, and PEC performance of binary heterostructured Bi_2S_3/ZnO NRAs/ITO.

2.3. Characterization of Bi_2S_3/ZnO Nanorod Arrays. FE-SEM measurements and energy dispersive X-ray (EDX) analysis of bare ZnO NRAs and Bi_2S_3/ZnO NRAs were carried out using JEOL JSM-7600F for morphological structure and elemental analysis. The structure, nature of crystalline phase, lattice fringe, and chemical composition were investigated by high-resolution transmission electron microscopy (HRTEM) with selected-area electron diffraction (SAED) and electron energy-loss spectroscopy (EELS) modes in the Tecnai TF20 x-twin FEI system, while X-ray diffraction (XRD) was used to characterize the crystal structure of the obtained thin films using a Philips PM1730 diffractometer (Panalytical X'Pert Pro MPD diffractometer) using Cu-Kα ($\lambda = 1.54$ Å) radiation at 40 kV and 40 mA at the range of $20^\circ<\theta<80^\circ$ with Panalytical X'Pert HighScore software. The scanning range was maintained within 20°-80° with a scanning speed of $5^\circ\,min^{-1}$. Raman spectroscopic analysis was conducted using Wissenschaftliche Instrument and Technology (WITec) Raman spectrometer, Alpha 300R (WITec GmbH, Ulm, Germany). The Raman frequency was acquired with laser excitation wavelength of 532 nm and an integration time of 5 sec. Absorbance spectra of prepared thin films were recorded using (UV-2600, Shimadzu) spectrophotometer in the range of wavelength between 300 and 800 nm. The PEC performance analysis was conducted in a three-electrode electrochemical cell configuration consisting of bare ZnO NRAs/ITO and Bi_2S_3/ZnO NRAs/ITO as the semiconductor working electrode and Pt wire as the counter electrode while Ag/AgCl electrode as the reference electrode. The measurement was carried out using linear sweep voltammetry (Autolab PGSTAT204/FRA32M module) to control the potential and recorded the corresponding photocurrent density at the scan rate of $20\,mVs^{-1}$ in a mixture of equimolar concentration of 0.1 M Na_2S and Na_2SO_3 electrolyte (pH = 13). The semiconductor electrodes were illuminated with chopped light using halogen lamp at an intensity of $100\,mWcm^{-2}$ in the visible region (400-800 nm) which was measured using fibre optic spectrometer (Avaspec-2048). The electrochemical impedance spectroscopy (EIS) measurements were measured under the illumination condition in the frequency range from 0.01 Hz to 1 MHz.

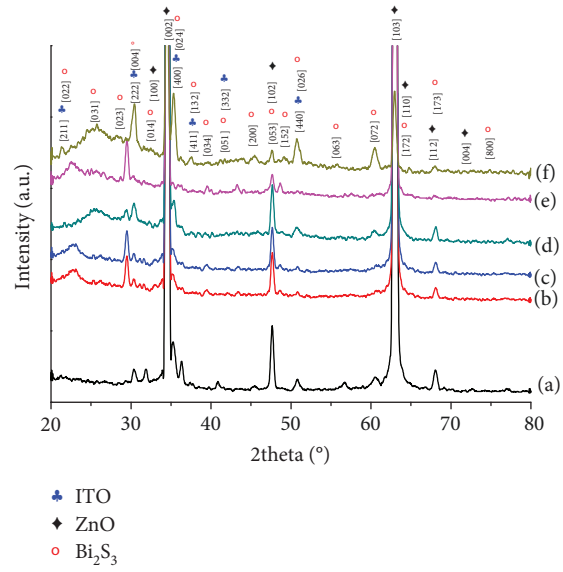

Figure 1: X-ray diffraction of ZnO NRs (a); Bi_2S_3/ZnO NRs/ITO at different SILAR cycles of (b) 3 cycles, (c) 5 cycles, (d) 7 cycles, (e) 9 cycles, and (f) 11 cycles.

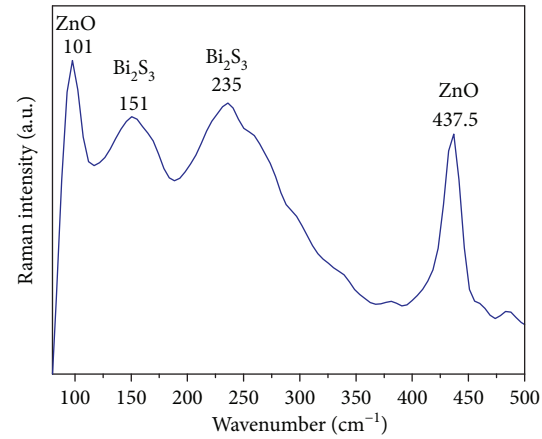

Figure 2: Raman spectrum of Bi_2S_3/ZnO NRs/ITO heterostructure at 7 SILAR cycles versus wavenumber.

3. Results and Discussion

The XRD pattern of ZnO NRAs/ITO and Bi_2S_3/ZnO NRAs/ITO heterostructure thin films prepared by the SILAR method as a function of SILAR cycles is presented in Figure 1. The XRD patterns of ZnO NRAs are well matched with the standard ZnO JCPDS: (00-003-0888). It was also noted that ZnO was in hexagonal structure and was strongly oriented along (002) which indicated the perpendicular growth of ZnO NRAs on ITO substrate. The diffraction peaks located at 2θ of 31.77°, 34.65°, 36.25°, 56.60°, and 62.86° are attributed to (100), (002), (102), (110), and (103). The additional peaks present in Bi_2S_3/ZnO NRAs/ITO film were shown to belong to Bi_2S_3 which was matched with JCPDS card (03-065-3884); the structure was noted to be orthorhombic [13]. Planes were observed along with (022), (031), (023), (004), (024), (132), (034), (051), (200), (053), (152), (026), (063), (072), and (172). Apart from these peaks, only indium tin oxide peaks were distinguished in all the samples coated on ITO substrate. Additionally, there was no remarkable shift in the diffraction peaks, other crystalline impurities were not observed, and the deposition of Bi_2S_3 occurred at different SILAR cycles. As this finding proves that the SILAR reaction is an efficient approach to form good crystallization heterostructure thin films, the peak intensity of Bi_2S_3 such as (022), (004), (024), (026), and (072) increased with increasing the SILAR cycle number which indicates that more Bi_2S_3 was deposited. Due to larger

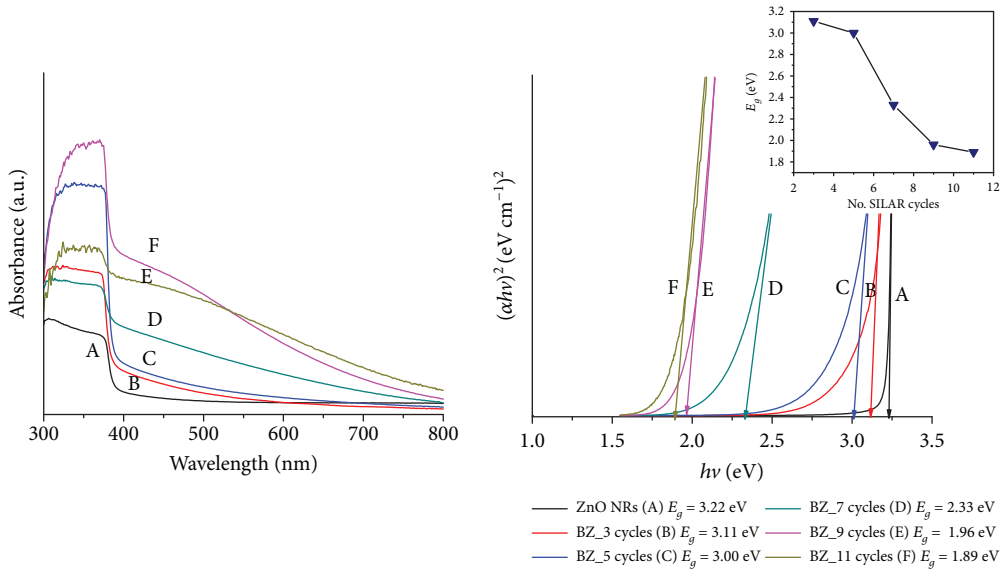

(a) (b)

Figure 3: (a) UV-Vis spectra; (b) band gap energy curves of (A) ZnO NRs/ITO and Bi_2S_3/ZnO NRAs/ITO prepared at different SILAR cycles (B) 3 cycles, (C) 5 cycles, (D) 7 cycles, (E) 9 cycles, and (F) 11 cycles, and the inset plot shows SILAR cycle number vs. change in optical band gap energy.

amount of Bi_2S_3, the intensity of ZnO peaks, such as (102) and (103), decreased accordingly.

Raman spectroscopy is considered one of the most powerful tools for the structural characterization of nanomaterials. Figure 2 shows the Raman spectrum of optimal Bi_2S_3/ZnO NRAs photoanode (i.e., at 7 cycles) deposited by the SILAR method. The Raman spectrum heterostructure displays two vibrations at approximately 437.5 cm^{-1} and 101 cm^{-1} corresponding to E_2-high phonon modes and E_2-low phonons of ZnO NRAs, respectively [28]. Additionally, two distinct Raman peaks at 151 cm^{-1} and 235 cm^{-1} attributed to Bi_2S_3 which are in a good agreement with two Raman bands reported earlier [29, 30].

The optical absorption spectra of grown ZnO NRs and Bi_2S_3/ZnO NRAs were recorded at different SILAR cycles as shown in Figure 3(a). It can be seen that bare ZnO NRs show low absorbance edge at around 385 nm with a band gap energy value of 3.22 eV, while the absorption spectrum of Bi_2S_3/ZnO shifted from blue to red and shows a combination of absorbance of ZnO and Bi_2S_3 thin film. As the cycles of Bi_2S_3 over ZnO NRs increased, the absorbance edge shifted to longer wavelength indicating a significant improvement in ZnO ability of harvesting the visible light spectrum.

The band gap energy was determined by using Tauc's relationship between the photon energy ($h\nu$) and the absorption coefficient (α) using the following equation [31]:

$$(\alpha h\nu) = A\left(h\nu - E_g\right)^n, \quad (1)$$

where α is the absorption coefficient, $h\nu$ is the energy of incident photon, A is constant, and E_g is the optical band gap energy (eV) while n depends on the type of transition ($n = 1/2$ and 2 for allowable direct and indirect transmission, respectively).

The semiconducting behaviour with direct band gap energy was confirmed via the linear variation of $(\alpha h\nu)^2$ against the photon energy at an absorption edge as demonstrated in Figure 3(b). The band gap energy values were calculated from extrapolating the straight-line portion of the plot $(\alpha h\nu)^2$ versus $(h\nu)$. The thickness of ZnO NRAs and Bi_2S_3/ZnO NRAs thin films was estimated using surface profiler (AMBIOS *XP*-200) and found to be 850.46 nm, 912.13 nm, 920.80 nm, 934.30 nm, 939.18 nm, and 944.06 nm for ZnO NRAs, Bi_2S_3/ZnO at 3, 5, 7, 9, and 11 SILAR cycles. The calculated band gap energy is 3.22, 3.11, 3.00, 2.33, 1.96, and 1.89 eV for plain ZnO NRAs, Bi_2S_3/ZnO at 3, 5, 7, 9, and 11 SILAR cycles, respectively. It is found that there is an optical absorption shifted to lower energy of Bi_2S_3/ZnO NRAs observed compared to that of bare ZnO NRAs confirming the enhancement of visible light harvesting for the obtained heterostructure.

The surface morphology of the obtained thin films was examined by using a field emission scanning electron microscopy (FE-SEM). Figure 4 shows the top view surface morphology of bare ZnO NRAs and Bi_2S_3/ZnO NRAs/ITO at two different magnifications. These micrographs show the hexagonal crystal of 30.07 nm of ZnO NRAs. Figure 4(b) depicts the decoration of small nanostructure of Bi_2S_3 on the whole surface of ZnO NRAs with comprehensive area coverage. The higher magnification shows how Bi_2S_3 nanoparticles distributed uniformly and coated homogeneously on ZnO NRAs without changing the structure of nanorods. The high magnification images (Figures 4(b)–4(d)) of Bi_2S_3/ZnO NRs at 3, 7, and 11 layers reveal that the surface

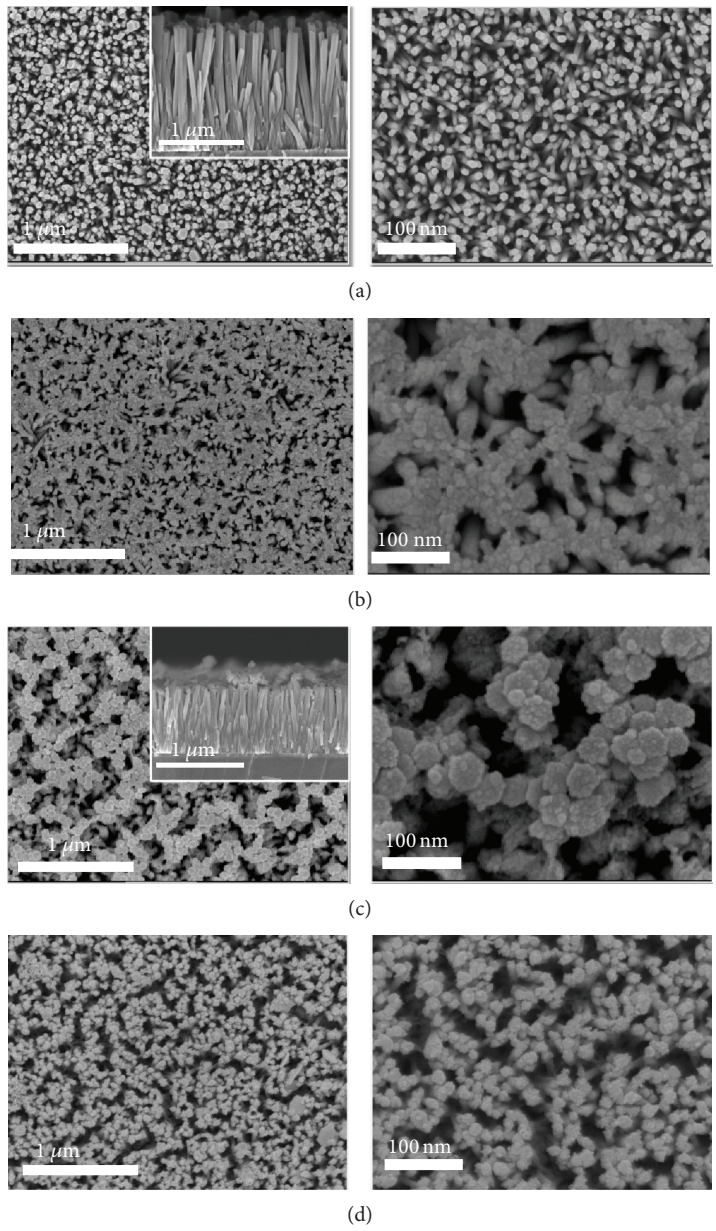

Figure 4: FE-SEM images of bare ZnO NRAs (a) at lower and higher magnification and ZnO nanorods decorated with Bi_2S_3 nanoparticles at lower and higher magnification, for (b) 3 cycles, (c) 7 cycles, and (d) 11 cycles. Cross-sectionals of the samples (a, c) are shown in the insets of the figures.

of ZnO NRs became rougher and was fully covered by Bi_2S_3 when the SILAR cycle was boosted from 3 to 7 cycles as shown in the cross-section inset (Figures 4(a) and 4(c)). When the SILAR cycles were increased to 11 cycles, there was an indicator of agglomeration as a result of increasing the amount of Bi_2S_3, which may have affected the space between ZnO NRs. Additionally, the EDX results show that the atomic percentage of Bi and S increased significantly when the SILAR cycles boosted from 3 to 7 cycles as illustrated in Figures 5(a) and 5(b). The ratio of Bi to S element is about 2 : 3 which thereby confirmed the deposition of stoichiometry Bi_2S_3. Thus, the results indicate that ZnO NRAs were successfully modified with Bi_2S_3 throughout the SILAR technique, without other element peaks detected which proved the excellent quality of the obtained sample. Figure 5(c) presents the corresponding element mapping (EELS) of the optimum sample (7 cycles) which can be found in the element of Zn, O, Bi, and S.

The detailed nanostructure was then analyzed using TEM and selected-area electron diffraction (SAED) as shown in Figure 6(a). TEM images of Bi_2S_3/ZnO NRs (7 cycles) were displayed in Figure 6(b) which confirms the homogeneous distribution of Bi_2S_3 nanoparticles, which can effectively sensitize ZnO NRs for photoresponse. Figure 6(c) displays the HR-TEM image of Bi_2S_3/ZnO NRs (7 cycles). The plane fringes with crystalline plane spacing of 0.26 and 0.31 of

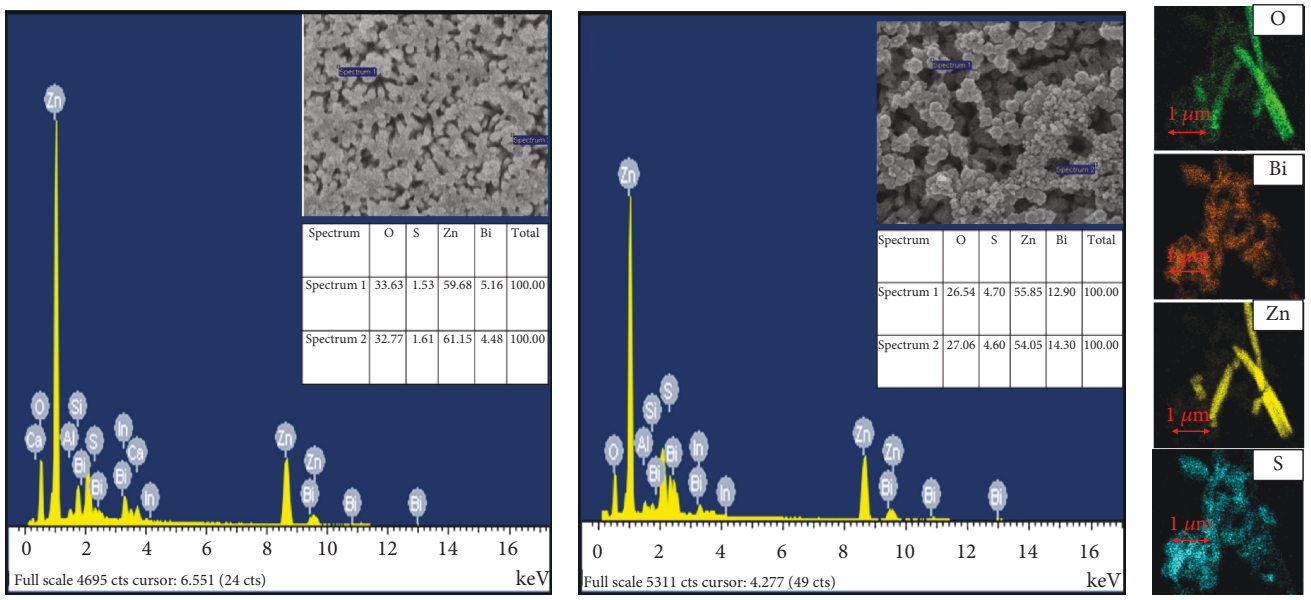

(a) (b) (c)

Figure 5: Energy dispersive X-ray (EDX) spectra of Bi_2S_3/ZnO NRAs/ITO heterostructure at (a) 3 cycles and (b) 7 cycles. (c) Elemental mapping EELS of Bi_2S_3/ZnO NRAs/ITO heterostructure (7 cycles). Inset shows the tabulated EDX data in atomic % of the corresponding films.

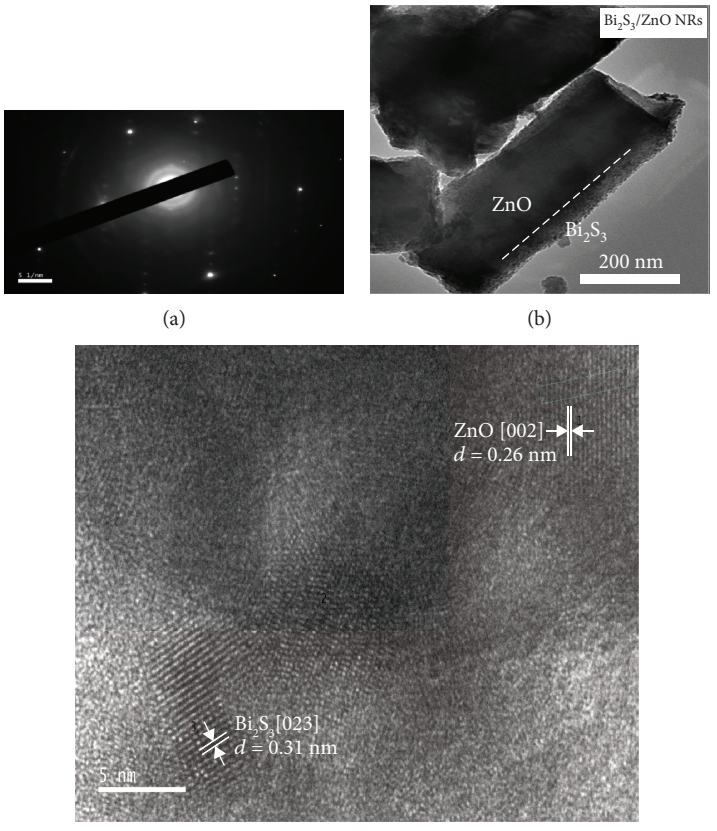

(a) (b) (c)

Figure 6: (a) The SAED pattern; (b) TEM image; (c) HRTEM image for the optimal sample Bi_2S_3/ZnO NRs (7 SILAR cycles).

wurtzite ZnO NRAs (002) and orthorhombic Bi_2S_3 (023), respectively. The results agreed well with XRD patterns which have been discussed previously (Figure 1).

3.1. Photoelectrochemical Performance. To study the photoelectrochemical performance of the Bi_2S_3/ZnO NRAs/ITO heterostructures at different SILAR cycles, it is important to find out the band edge potential of both Bi_2S_3 and ZnO as band edge potentials play a significant role in determining the migration routes of photoinduced electrons and holes. Additionally, the photoconversion efficiency depends on optical absorption, morphological structure, separation efficiency, transportation speed, and recombination rate of photogenerated charge carriers [24]. Figure 7 demonstrates the schematic diagram of band alignment of Bi_2S_3/ZnO NRA heterostructure. From this diagram, it may be observed that the Fermi level of Bi_2S_3 and ZnO is aligned, and the conduction band and valence band of Bi_2S_3 are higher than the conduction band and valence band of ZnO. The high valence band of Bi_2S_3 facilitated the transformation of the photogenerated electron when Bi_2S_3/ZnO NRAs/ITO heterostructured working electrode was irradiated. The immigration of the photogenerated electron from the conduction band of Bi_2S_3 to the conduction band of ZnO NRAs signified that more photogenerated electrons clustered at the active site area, consequently increasing the photocurrent density remarkably.

Figure 8 demonstrates the linear sweep voltammograms (LSVs) of bare ZnO NRAs and Bi_2S_3/ZnO NRAs/ITO at different SILAR cycles. It could be noticed that the photocurrent density improved significantly after coating Bi_2S_3 on ZnO NRAs due to the obtained enhancement in the charge separation and charge carrier transportation and the lowering of the recombination rate. It is noticed that the photocurrent density is higher in the heterostructured photoanode compared to the bare semiconductor, owing to the effective charge separation and the mobility of electrons. Apart from the impact of SILAR cycles on the PEC performance, the results revealed that the photocurrent density increased remarkably when the SILAR cycles increased from 3 to 7 cycles as a result of increasing the amount of Bi_2S_3 deposit on ZnO NRs uniformly before showing reduction for further cycles. The lesser photocurrent due to the increment of photogenerated electron resistance and delayed penetration of multisulphide electrolyte in the thin film was a result of agglomeration of small size of Bi_2S_3 on ZnO NRs which reduced the spaces between the nanorods [32]. Moreover, the increasing of the SILAR cycles formed cluster of Bi_2S_3 which might block the light from penetrating through to the irradiated ZnO NRAs. This reduction indicates that recombination process occurred, and the photogenerated holes reached the surface instead of arresting electrons from electrolyte accumulating at ITO surface and recombining with electrons from the conduction band [26].

The significant enhancement in PEC performance for Bi_2S_3/ZnO NRAs/ITO heterostructure may also be explained based on the electrochemical impedance spectra (EIS), which evaluate the mechanism of interfacial charge transfer process, implying the influence of charge separation and recombination rate. Besides, it is also an important evidence on the correlation between photoconversion efficiency and charge transfer. EIS was also conducted under visible light illumination. Figure 9 demonstrates the EIS Nyquist plot of bare ZnO NRAs/ITO and Bi_2S_3/ZnO NRAs/ITO at 7 cycles. The arc portion assigned to the charge transform as well as the recombination rate between the photoanode and the electrolyte is also illustrated in this plot. The intercept on the real axis of the Nyquist plot corresponds to the charge transfer resistance (R_{ct}) at the interface [33]. The small R_{ct} of the heterostructure (699 Ω) compared to bare ZnO NRAs (11990 Ω) indicates the prolonged lifetime of the photogenerated electron after coating Bi_2S_3/ZnO NRs and faster interfacial charge transfer as well as a low recombination rate. It is concluded that Bi_2S_3 with narrow band gap energy acts as a highway to facilitate charge carrier transportation. The system with low charge transformation resistance leads to the significant improvement in PEC performance.

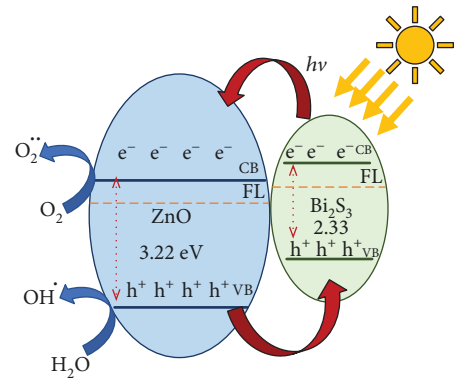

FIGURE 7: Schematic band alignment of structure Bi_2S_3/ZnO NRA binary nanostructure under illumination.

The photoconversion efficiency (η%) of photoenergy to chemical energy is estimated using the following equation [34]:

$$\eta = \frac{J_{ph(1.23-V_{app})}}{P_{in}} \times 100\%, \quad (2)$$

where J_{ph} ($J_{ph} = J_{light} - J_{dark}$) refers to the obtained photocurrent density in (mA/cm^2); V_{app} (V) refers to the voltage applied to photoanode versus Ag/AgCl. The water electrolysis's standard reversible redox potential (as compared to the normal hydrogen electrode (NHF)) could be represented as 1.23 V. Meanwhile, P_{in} refers to the power intensity of illumination source (mWcm^{-2}). The highest value of the photoconversion efficiency achieved was 1.67% for Bi_2S_3/ZnO NRAs, fabricated at 7 SILAR cycles compared to bare ZnO NRAs/ITO (0.25%), as illustrated in Figure 10. Thus, Bi_2S_3/ZnO NRA (7cycles) electrode provides approximately 7 times greater photoconversion efficiency compared to ZnO NRA electrode. This is due to the uniform deposition of Bi_2S_3 nanoparticles (7cycles) onto ZnO NRAs that contributed in efficient absorption of visible light. The value of photoconversion efficiency improved impressively (67 times)

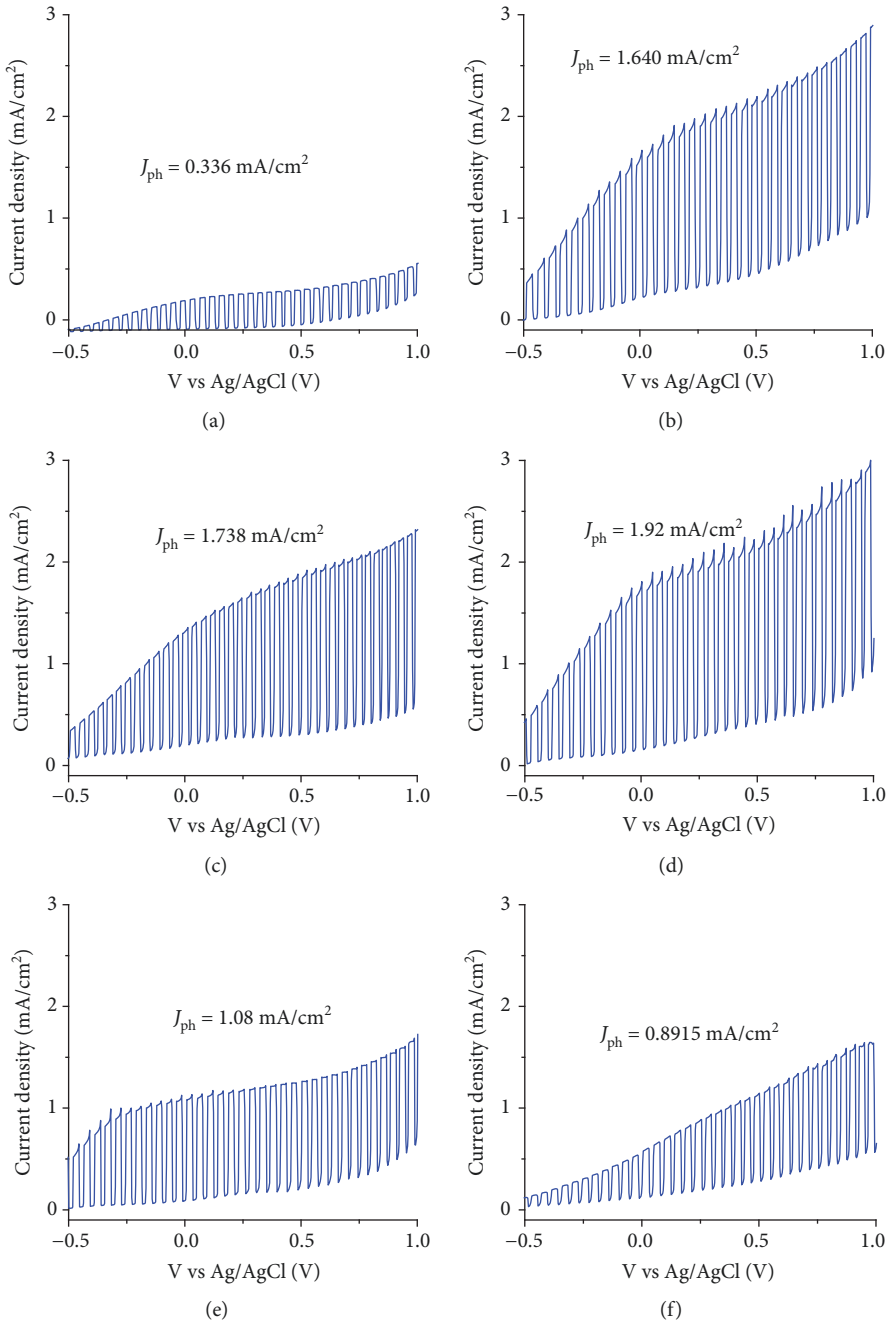

FIGURE 8: Linear sweep voltammograms obtained at the scan rate of 20 mV s^{-1} at applied potentials from -0.5 V to +1.0 V under illumination intensity of 100 mWcm^{-2} in 0.1 M Na_2S and Na_2SO_3 electrolyte for (a) bare ZnO NRAs/ITO; Bi_2S_3/ZnO NRAs/ITO at different SILAR cycle numbers: (b) 3 cycles; (c) 5 cycles; (d) 7 cycles; (e) 9 cycles; (f) 11 cycles.

compared to previous report [26]. It can be concluded that Bi_2S_3 prepared at 7 SILAR cycles may be introduced as an excellent photosensitizer for ZnO NRAs.

4. Conclusion

Systemic investigation has been directed towards the optimization of the surface of ZnO NRAs with Bi_2S_3 by the SILAR technique. The variation in SILAR cycles for Bi_2S_3 and its effect on the optical and morphological structure and photoconversion efficiency was investigated extensively. The orthorhombic phase of Bi_2S_3 over the wurtzite structure of ZnO was proven throughout XRD results. The optical properties of ZnO NRAs improved significantly after sensitizing by Bi_2S_3, and the band gap energy decreased by increasing the coating cycles. The enhancement in the photoconversion efficiency was observed for Bi_2S_3/ZnO NRAs/ITO at 7 cycles (1.67%) to that of bare ZnO NRs/ITO (0.25%), due to the reduction of the electrical impedance of Bi_2S_3/ZnO NRAs as proven by EIS measurements. This fundamental

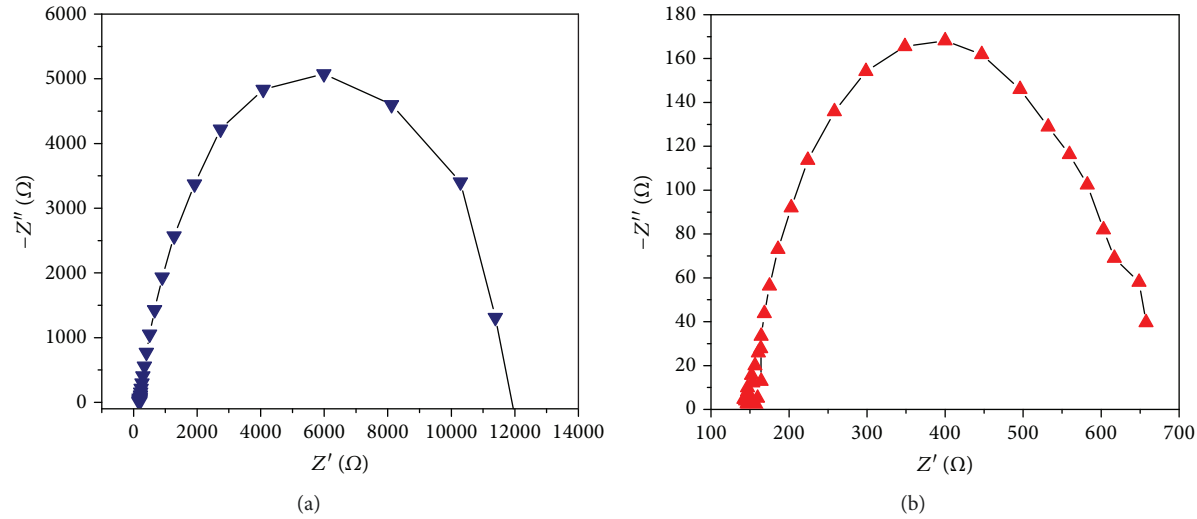

Figure 9: EIS Nyquist plot of (a) bare ZnO NRAs/ITO; (b) Bi_2S_3/ZnO NRAs/ITO at 7 SILAR cycles at open bias condition under visible light illumination.

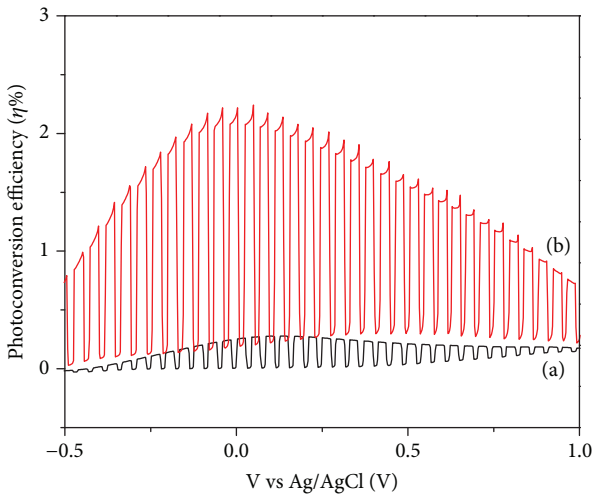

Figure 10: Photoconversion efficiency as a function of applied voltage versus Ag/AgCl of (a) bare ZnO NRAs/ITO; (b) Bi_2S_3/ZnO NRAs prepared at 7 SILAR cycles under illumination intensity of 100 $mWcm^{-2}$ in 0.1 M Na_2SO_3 and 0.1 M Na_2S electrolyte mixture.

result confirms the effectiveness of utilizing coated ZnO nanorods towards the improvement of photoelectrochemical cell performance. Besides, it opens the new and simplified technique towards utilizing the abundant visible spectrum and the development of the PEC material at low cost.

Data Availability

The data used to support the findings of this study are included within the article.

Conflicts of Interest

The authors declare that they have no conflicts of interest.

Acknowledgments

This work is funded by the Ministry of Higher Education of Malaysia via the grant FRGS (01-01-17-1912FR). The authors would also like to gratefully acknowledge Saudi Culture Mission for their financial support to Asla Abdullah Al-Zahrani. Special thanks are also extended to the Department of Chemistry and Department of Physics, Faculty of Science, Universiti Putra Malaysia, and Microscopy Unit, Institute of Bioscience, Universiti Putra Malaysia, for providing the facilities and equipment required for this study.

Supplementary Materials

The detailed experimental design of ZnO nanoparticles, ZnO nanorods, and heterostructured Bi_2S_3/ZnO NRAs was available in the supplementary materials. *(Supplementary Materials)*

References

[1] Y. Y. Lou, S. Yuan, Y. Zhao, Z.-Y. Wang, and L.-Y. Shi, "Influence of defect density on the ZnO nanostructures of dye-sensitized solar cells," *Advances in Manufacturing*, vol. 1, no. 4, pp. 340–345, 2013.

[2] Y. Zhang, Y. Liu, L. Zhou et al., "The role of Ce doping in enhancing sensing performance of ZnO-based gas sensor by adjusting the proportion of oxygen species," *Sensors and Actuators B: Chemical*, vol. 273, pp. 991–998, 2018.

[3] S. A. Patil, Y. T. Hwang, V. V. Jadhav, K. H. Kim, and H. S. Kim, "Solution processed growth and photoelectrochemistry of Bi_2S_3 nanorods thin film," *Journal of Photochemistry and Photobiology A: Chemistry*, vol. 332, pp. 174–181, 2017.

[4] D. P. Norton, Y. W. Heo, M. P. Ivill et al., "ZnO: growth, doping & processing," *Materials Today*, vol. 7, no. 6, pp. 34–40, 2004.

[5] A. Helal, F. A. Harraz, A. A. Ismail, T. M. Sami, and I. A. Ibrahim, "Hydrothermal synthesis of novel heterostructured Fe_2O_3/Bi_2S_3 nanorods with enhanced photocatalytic activity

under visible light," *Applied Catalysis B: Environmental*, vol. 213, pp. 18–27, 2017.

[6] Ü. Özgür, D. Hofstetter, and H. Morkoç, "ZnO devices and applications: a review of current status and future prospects," *Proceedings of the IEEE*, vol. 98, no. 7, pp. 1255–1268, 2010.

[7] P. R. Nikam, P. K. Baviskar, J. V. Sali, K. V. Gurav, J. H. Kim, and B. R. Sankapal, "CdS surface encapsulated ZnO nanorods: synthesis to solar cell application," *Journal of Alloys and Compounds*, vol. 689, pp. 394–400, 2016.

[8] X. Li, J. Li, C. Cui, Z. Liu, and Y. Niu, "PbS nanoparticle sensitized ZnO nanowire arrays to enhance photocurrent for water splitting," *The Journal of Physical Chemistry C*, vol. 120, no. 8, pp. 4183–4188, 2016.

[9] A. M. Holi, Z. Zainal, A. K. Ayal et al., "Effect of heat treatment on photoelectrochemical performance of hydrothermally synthesised Ag_2S/ZnO nanorods arrays," *Chemical Physics Letters*, vol. 710, pp. 100–107, 2018.

[10] L. Tang, Y. Deng, G. Zeng et al., "CdS/Cu_2S co-sensitized TiO_2 branched nanorod arrays of enhanced photoelectrochemical properties by forming nanoscale heterostructure," *Journal of Alloys and Compounds*, vol. 662, pp. 516–527, 2016.

[11] O. Messaoudi, H. Makhlouf, A. Souissi et al., "Synthesis and characterization of ZnO/Cu_2O core–shell nanowires grown by two-step electrodeposition method," *Applied Surface Science*, vol. 343, pp. 148–152, 2015.

[12] P. R. Nikam, P. K. Baviskar, S. Majumder, J. V. Sali, and B. R. Sankapal, "SILAR controlled CdSe nanoparticles sensitized ZnO nanorods photoanode for solar cell application: electrolyte effect," *Journal of Colloid and Interface Science*, vol. 524, pp. 148–155, 2018.

[13] S. Velanganni, A. Manikandan, J. J. Prince, C. N. Mohan, and R. Thiruneelakandan, "Nanostructured ZnO coated Bi_2S_3 thin films: enhanced photocatalytic degradation of methylene blue dye," *Physica B: Condensed Matter*, vol. 545, pp. 383–389, 2018.

[14] C. Liu, Y. Yang, W. Li, J. Li, Y. Li, and Q. Chen, "A novel Bi_2S_3 nanowire @ TiO_2 nanorod heterogeneous nanostructure for photoelectrochemical hydrogen generation," *Chemical Engineering Journal*, vol. 302, pp. 717–724, 2016.

[15] K. Yao, W. W. Gong, Y. F. Hu, X. L. Liang, Q. Chen, and L. M. Peng, "Individual Bi_2S_3 nanowire-based room-temperature H_2 sensor," *The Journal of Physical Chemistry C*, vol. 112, no. 23, pp. 8721–8724, 2008.

[16] R. D. Ladhe, P. K. Baviskar, S. M. Pawar, J. H. Kim, and B. R. Sankapal, "The n-Bi_2S_3/p-PbS heterojunction for room temperature LPG sensors," *Sensors and Actuators A: Physical*, vol. 267, pp. 187–193, 2017.

[17] G. Konstantatos, L. Levina, J. Tang, and E. H. Sargent, "Sensitive solution-processed Bi_2S_3 nanocrystalline photodetectors," *Nano Letters*, vol. 8, no. 11, pp. 4002–4006, 2008.

[18] M. Han and J. Jia, "3D Bi_2S_3/TiO_2 cross-linked heterostructure: an efficient strategy to improve charge transport and separation for high photoelectrochemical performance," *Journal of Power Sources*, vol. 329, pp. 23–30, 2016.

[19] J. Arumugam, A. D. Raj, A. A. Irudayaraj, and M. Thambidurai, "Solvothermal synthesis of Bi_2S_3 nanoparticles and nanorods towards solar cell application," *Materials Letters*, vol. 220, pp. 28–31, 2018.

[20] X. Yang, S. Tian, R. Li, W. Wang, and S. Zhou, "Use of single-crystalline Bi_2S_3 nanowires as room temperature ethanol sensor synthesized by hydrothermal approach," *Sensors and Actuators B: Chemical*, vol. 241, pp. 210–216, 2017.

[21] S. Balachandran and M. Swaminathan, "The simple, template free synthesis of a Bi_2S_3–ZnO heterostructure and its superior photocatalytic activity under UV-A light," *Dalton Transactions*, vol. 42, no. 15, pp. 5338–5347, 2013.

[22] A. N. Kulkarni, M. B. Rajendra Prasad, H. M. Pathan, and R. S. Patil, "TiO_2 photoanode sensitized with nanocrystalline Bi_2S_3: the effect of sensitization time and annealing on its photovoltaic performance," *Applied Nanoscience*, vol. 6, no. 4, pp. 567–574, 2016.

[23] S. Kumar, S. Sharma, A. Umar, and S. K. Kansal, "Bismuth sulphide (Bi_2S_3) nanotubes as an efficient photocatalyst for methylene blue dye degradation," *Nanoscience and Nanotechnology Letters*, vol. 8, no. 3, pp. 266–272, 2016.

[24] M. Han and J. Jia, "The interlace of Bi_2S_3 nanowires with TiO_2 nanorods: an effective strategy for high photoelectrochemical performance," *Journal of Colloid and Interface Science*, vol. 481, pp. 91–99, 2016.

[25] C. Tang, Y. Zhang, J. Su et al., "Synthesis and photocatalytic properties of vertically aligned Bi_2S_3 platelets," *Solid State Sciences*, vol. 51, pp. 24–29, 2016.

[26] P. R. Nikam, P. K. Baviskar, J. V. Sali, K. V. Gurav, J. H. Kim, and B. R. Sankapal, "SILAR coated Bi_2S_3 nanoparticles on vertically aligned ZnO nanorods: synthesis and characterizations," *Ceramics International*, vol. 41, no. 9, pp. 10394–10399, 2015.

[27] V. V. Killedar, S. N. Katore, and C. H. Bhosale, "Preparation and characterization of electrodeposited Bi_2S_3 thin films prepared from non-aqueous media," *Materials Chemistry and Physics*, vol. 64, no. 2, pp. 166–169, 2000.

[28] A. F. Abdulrahman, S. M. Ahmed, and M. A. Almessiere, "Effect of the growth time on the optical properties of ZnO nanorods grown by low temperature method," *Digest Journal of Nanomaterials and Biostructures*, vol. 12, no. 4, pp. 1001–1009, 2017.

[29] C. Tang, C. Wang, F. Su et al., "Controlled synthesis of urchin-like Bi_2S_3 via hydrothermal method," *Solid State Sciences*, vol. 12, no. 8, pp. 1352–1356, 2010.

[30] Y. Wang, J. Chen, L. Jiang, K. Sun, F. Liu, and Y. Lai, "Photoelectrochemical properties of Bi_2S_3 thin films deposited by successive ionic layer adsorption and reaction (SILAR) method," *Journal of Alloys and Compounds*, vol. 686, pp. 684–692, 2016.

[31] J. Tauc, R. Grigorovici, and A. Vancu, "Optical properties and electronic structure of amorphous germanium," *Physica Status Solidi (b)*, vol. 15, no. 2, pp. 627–637, 1966.

[32] S. K. Kokate, A. T. Supekar, P. K. Baviskar et al., "CdS sensitized pristine and Cd doped ZnO solar cells: effect of SILAR cycles on optical properties and efficiency," *Materials Science in Semiconductor Processing*, vol. 80, pp. 179–183, 2018.

[33] M. Z. Iqbal and S. Siddique, "Recent progress in efficiency of hydrogen evolution process based photoelectrochemical cell," *International Journal of Hydrogen Energy*, vol. 43, no. 46, pp. 21502–21523, 2018.

[34] D. Kumar, R. Bai, S. Chaudhary, and D. K. Pandya, "Enhanced photoelectrochemical response for hydrogen generation in self-assembled aligned ZnO/PbS core/shell nanorod arrays grown by chemical bath deposition," *Materials Today Energy*, vol. 6, pp. 105–114, 2017.